Letter

Experimental validation of a micromechanically based compaction law for mixtures of soft and hard grains

Manuel Cárdenas-Barrantes,[1,*] Jonathan Barés,[1,†] Mathieu Renouf,[1,‡] and Émilien Azéma[1,2,§]
[1]*Laboratoire de Mécanique et Génie Civil, UMR 5508 CNRS, University Montpellier, 34095 Montpellier, France*
[2]*Institut Universitaire de France, 75231 Paris, France*

(Received 2 November 2021; accepted 16 June 2022; published 3 August 2022)

In this Letter, we report on an experimental study which analyzes the compressive behavior of two-dimensional bidisperse granular assemblies made of soft (hyperelastic) and hard grains in varying proportions (κ is the portion of soft grains). By means of a recently developed uniaxial compression setup [Vu and Barés, Phys. Rev. E **100**, 042907 (2019)] and using an advanced digital image correlation method, we follow, beyond the jamming point, the evolution of the main mechanical observables, from the global scale down to the strain field inside each deformable grain. First, we validate experimentally and extend to the uniaxial case a recently proposed micromechanical compaction model linking the evolution of the applied pressure P to the packing fraction ϕ [Cantor *et al.*, Phys. Rev. Lett. **124**, 208003 (2020)]. Second, we reveal two different linear regimes depending on whether the system is above or below a crossover strain unraveling a transition from a discrete to a continuous-like system. Third, the evolution of these linear laws is found to vary linearly with κ. These results provide a comprehensive experimental and theoretical framework that can now be extended to a more general class of polydisperse soft granular systems.

DOI: 10.1103/PhysRevE.106.L022901

Granular materials are ubiquitous in nature and human activities. In their most generic form, they are composed of grains of shape, dimension, and, more importantly, bulk properties that are very different, even in the same packing. Among them, granular systems composed of squeezable compounds are the ones with the most singular behaviors. This is the case for biological tissues composed of soft cells [1,2], liquid foams [3,4], emulsions [5,6], and sintered material [7,8], to name a few. The specificity of materials composed of both soft and hard particles lies in the fact that under any loading, and even deep in the jammed state [9], two mechanisms compete in the system: particle rearrangement and deformation. When loaded, hard particles have only the ability to rearrange abruptly [10,11], while it is easier for soft particles to deform in order to sustain a given strain [12]. In these materials, both mechanisms cohabit, prioritizing one or the other depending on the soft to hard particle ratio and global loading.

Compressed systems made of purely hard or slightly deformable particles have been extensively studied these last decades from theoretical [9,13–15], numerical [16,17], and experimental [18–20] points of view. Most of the fundamental aspects of their behavior in many circumstances are now well known [9,14,21]. The behavior of systems made of highly deformable grains at high packing fraction has also been more and more studied [5,6,12,22,23], and at least for compaction, reliable models exist [24,25]. In between, even if they are very common materials, systems composed of grains with very different—soft and hard—rheologies, driven far above the jamming transition, have a bewildering but fascinating behavior that remains mostly misunderstood. They have been experimentally studied in very specific applications, such as stress release [26,27], seismic isolation [28,29], and foundation damping [30,31]. However, to the best of our knowledge, no local measurements have been performed to understand the microprocesses leading to their characteristic macroscopic behavior. Only very recently, through a numerical approach, was a micromechanical-based compaction model proposed [22,23] to describe the evolution of these systems in compression. However, experimental validation is still lacking, along with a clear understanding of local processes.

In this Letter, we aim to fill this gap by extending the recently proposed compaction law [32], and experimentally validating it and, by stating constitutive laws, linking both local structural parameters and local strain field with global observables such as pressure and packing fraction. The evolution of these laws as a function of the fraction of soft grains is also investigated.

Experiment. The experiments were carried out using a setup partially introduced by [12,33]. As shown in Fig. 1(a), it consists of a bidimensional piston with initial dimensions of 270×202 mm^2 which uniaxially compresses a bidisperse collection of rigid and soft cylinders lying on top of a flatbed scanner. The loading piston is composed of a stepper motor rotating a screw which translates the moving edge of the piston in the inward direction. Two force sensors are attached to the latter. They record the global force f evolution [see Fig. 1(c)] when compressing the granular media. The induced global stress P is directly deduced and measured continuously

*manuel-antonio.cardenas-barrantes@umontpellier.fr
†jonathan.bares@umontpellier.fr
‡mathieu.renouf@umontpellier.fr
§emilien.azema@umontpellier.fr

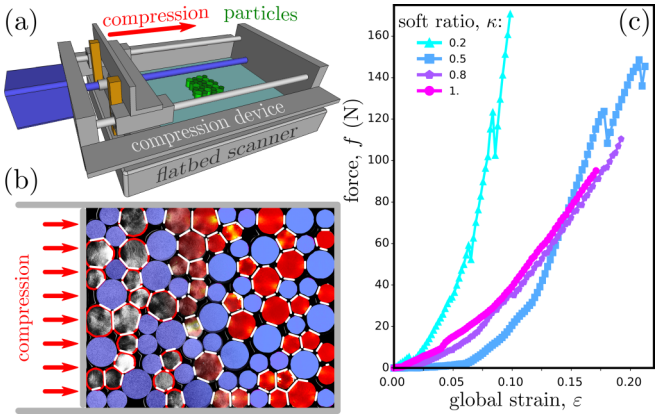

FIG. 1. (a) Experimental setup. A bidimensional bidisperse granular system, composed of soft and rigid particles, lies on the top glass of a flatbed scanner. A uniaxial compression device stresses it stepwisely while it is imaged from below by the scanner. (b) Composite view of measured fields. Rigid particles are colored in blue. Raw image, in gray, is shown on the left; particle boundaries are in red. Von Mises strain field $\mathcal{C}$ is shown on the right with a color scale going from dark red (low value) to yellow (high value). Contacts are shown in white. (c) Evolution of the measured global force f as a function of the global strain ε for different softness ratios κ.

at a frequency of 100 Hz, while the system is compressed stepwisely. For each loading step, the piston moves 0.5 mm at a speed of 2 mm/min to stay in the quasistatic regime. Then, the system relaxes for 1 min and is imaged from below with the scanner [34] at a resolution of 2400 dots per inch (10.6 μm/pixel).

The compressed granular systems are composed of both hyperelastic silicone cylinders [35,36] and rigid PVC cylinders. Their Young's moduli are $E_0 = 0.45$ MPa [37] and 1.2 GPa, respectively, and the Poisson ratio of silicone is $\nu = 0.5$. Both soft and rigid granular packings are bidisperse cylinders with diameters of 20 and 30 mm and a height of 15 mm. For each experiment, about $n = 100$ particles are used; the ratio between the rigid and soft ones is the *softness ratio*, $\kappa = n_{\text{soft}}/n$. This ratio is equally spread among soft and rigid particles and is varied from 0.2 to 1. To avoid basal friction the scanner glass is coated with oil [33]. This makes friction between any parts of the system less than 0.1. The bottom of each particle is coated with thin metallic glitter, which creates a random pattern with a correlation length of about 50 μm [12].

For each experiment, a set of about 90 pictures of ~500 megapixels displays the evolution of the bottom face of the granular system. These pictures are postprocessed with an algorithm modified from [12,38]. First, particles are detected individually by thresholding the undeformed picture. Each particle is then tracked along the full set of pictures. Then, from the particle's solid rigid motion measurement, subsets of images are extracted following each particle and correcting its translation and rotation. For soft particles, a digital image correlation (DIC) algorithm aimed at large deformations already presented in [37] is used to obtain the displacement field $\vec{u}$ inside each particle. For the rigid particles, a more classical DIC algorithm is used. The latter correlates all images with the initial one as classically done in the small deformation assumption.

As shown in Fig. 1(b), the particle boundaries are obtained from the displacement fields $\vec{u}$ [12]. The system packing fraction is directly deduced from it, along with the particle asphericity, $a = p^2/(4\pi s)$, where p and s are the perimeter and surface of the particles, respectively. For the soft particles, the right Cauchy-Green strain tensor field $\vec{\vec{C}}$ is computed [12,39], and its von Mises measure $\mathcal{C}$ is deduced [32]. For the rigid particles, the local stresses are too low to induce any significant deformation of the PVC [33]. Contacts between particles and their length l are measured from the proximity of the boundaries and the von Mises strain [12].

Finally, because the system size is relatively small, it is more sensitive to the initial conditions and sample preparation. To limit this effect, we paid particular attention to preparing the system as homogeneously as possible, which is usually done when preparing experimental or numerical samples [40–42], minimizing the vicinity of particles of the same size and rigidity. Moreover, the mean behavior for each κ is averaged over three different samples with initially independent configurations. Note that the systems were prepared loosely enough to observe the jamming transition [9]. This lets some space for the system to rearrange and somehow forget the initial conditions. The way to select the packing fraction ϕ_J at the jamming transition and the corresponding mean coordination number Z_J are discussed in more detail in the Supplemental Material [32].

Results. In Fig. 2(a), we show how the increase in the coordination from the jamming point $Z - Z_J$ evolves with the relative packing fraction $\phi - \phi_J$. Whatever the softness ratio is, curves collapse on a single one fitted by a power law with exponent $\alpha = 0.5$ and prefactor $k = 4.9$, in agreement with previous experimental and numerical observations [36,43,44]. Thus, our experimental results extend the validity of such a relation to the case of binary mixtures [22].

Following a recent micromechanical compaction model numerically tested on isotropically compressed soft grains [22,24,25], we extended it to the case of uniaxial compression [32]. In Fig. 2(b), compaction curves (P vs $\phi - \phi_J$) are plotted with

$$P \simeq \frac{E^*}{4\Gamma}(1+\mu_M)\frac{\phi_{\max}-\phi_J}{\phi_J}[Z_0 + k(\phi-\phi_J)^{0.5}]\phi \times \ln\left(\frac{\phi_{\max}-\phi_0}{\phi_{\max}-\phi}\right), \quad (1)$$

where $E^* = E_0/[2\kappa(1-\nu^2)]$ is the mean effective material Young's modulus and $\phi_{\max}$ is the asymptotic maximum packing fraction. For $\kappa = 1$, $\phi_{\max} = 0.97$ is close to 1, while for $\kappa = 0.2$, $\phi_{\max} = 0.88$, closer to the random close packing [32]. Γ is a geometrical parameter directly measured on the local vs global strain curve [32]. μ_M is the macroscopic friction known to be close to 0.25 for an assembly of two-dimensional particles [45,46]. The prediction given by Eq. (1) is in good agreement for all κ values. We note only a small discrepancy with experimental data at small κ, arising when the grains sharply rearrange. Even if the behavior is averaged over several runs, this effect is certainly enhanced by the fact that the system is relatively small. Finally, it should be noted

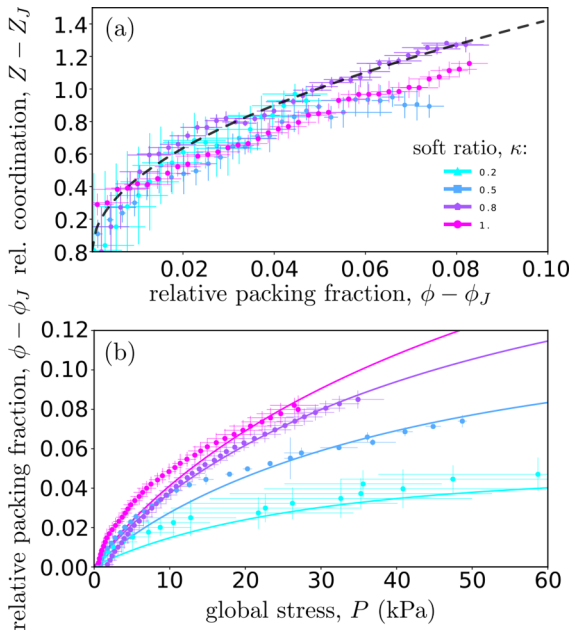

FIG. 2. (a) Evolution of the coordination Z relative to the coordination at jamming Z_J as a function of the distance to the jamming transition for the packing fraction $\phi - \phi_J$. The dashed line corresponds to a power law with an exponent 0.5. (b) Evolution of the global stress applied to the system P as a function of $\phi - \phi_J$. Plane line curves correspond to Eq. (1). In both panels, the different curves correspond to different softness ratios κ given in (a).

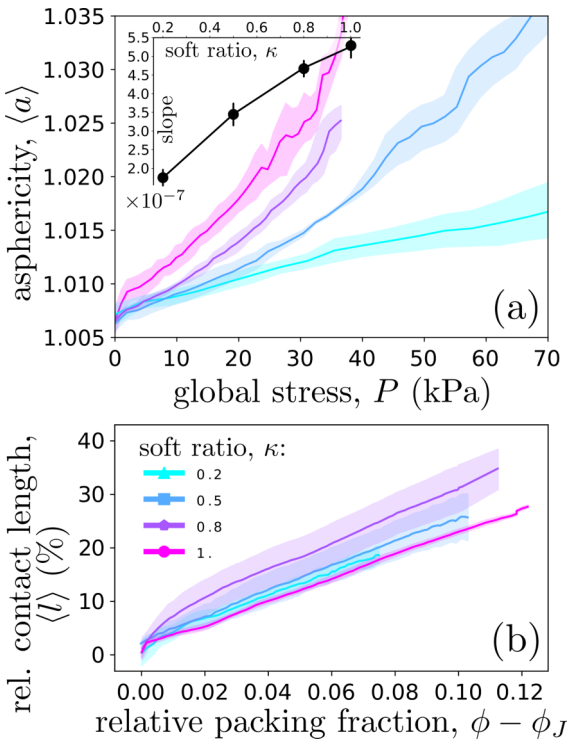

FIG. 3. (a) Linear evolution of the soft particle average asphericity $\langle a \rangle$ as a function of the global stress applied to the system P. Their slope is given in the inset as a function of the softness ratio κ. (b) Linear evolution of the average value of the relative contact length $\langle l \rangle$ as a function of the distance to the jamming transition for the packing fraction $\phi - \phi_J$. In both panels, the different curves correspond to different κ, given in the legend in (b).

that Eq. (1) is based on only well defined quantities without the need for any *ad hoc* parameters.

Figure 3(a) shows how the average soft particle asphericity $\langle a \rangle$ increases with the global stress P. Apart from a few sharp grain rearrangements, this increase is linear whatever the softness ratio κ is. The slope increases nearly linearly with κ. In Fig. 3(b) we show the evolution of the average relative contact length $\langle l \rangle$. It increases linearly with the packing fraction for any κ and, interestingly, with a slope independent of κ.

Under the small deformation assumption, the infinitesimal strain tensor $\vec{\vec{\varepsilon}}$ is related to $\vec{\vec{C}}$ following $\vec{\vec{\varepsilon}} = 1/2(\vec{\vec{C}} - \vec{\vec{I}})$, with $\vec{\vec{I}}$ being the second order identity tensor. Hence, as shown in Figs. 4(a) and 4(b), when the system is compressed, $\mathcal{C}$ decreases from 1, while the pressure and the packing fraction increase. At a low compression level, for $\langle \mathcal{C} \rangle \gg \mathcal{C}_c \approx 0.991$, a crossover strain, the average von Mises strain $\langle \mathcal{C} \rangle$, decreases linearly with the packing fraction. In this regime, whatever the softness ratio is, curves collapse fairly well. On the contrary, at high compression level, for $\langle \mathcal{C} \rangle < \mathcal{C}_c$, it decreases linearly with the global pressure. Not only does the average strain evolve during compression, but its distribution also gets wider [12,32]. In Fig. 4(c), we show how the standard deviation of $\mathcal{C}$ increases with the packing fraction. When shifted from ϕ_J, curves collapse on a linear law whatever κ is, up to a cutoff which increases linearly with κ.

Discussion and conclusion. First, we point out that, even if the system seems to be small, macroscopic measurements stay repeatable. The exponent α of the $Z - Z_J$ vs $\phi - \phi_J$ power law is repeatable from one κ value to another and fully in agreement with previous experimental and numerical studies [22–25,36,43]. As explained in [22,25], this law can be plugged into existing models to obtain an isotropic compaction equation. In the specific case of grain mixture, κ is introduced in the effective Young's modulus to consider the softness variation. Also, to consider the uniaxiality of the compression [47], the induced effective friction is added to the law prefactor to obtain Eq. (1) and describe the compaction curve without any *ad hoc* parameters. In this equation, $\phi_{\max}$ goes ideally from 1 for purely soft systems to ϕ_J for purely rigid systems, which is what we observe in our experimental data. So it is here remarkable that this model matches well the experimental data whatever the grain mixture is. This constitutes a validation of the model.

On top of extending and validating this compaction model, we introduce relations between global observables and deformed local structures. Hence, linear relations are observed between the particle asphericity and the global pressure ($\langle a \rangle \sim P$) as well as for the relative contact length and the packing fraction [$\langle l \rangle \sim (\phi - \phi_J)$]. This first observation permits indirect measurement of pressure in a granular system just by measuring the grain boundary deformations. For this latter linear relation, in the small deformation regime, a scaling consideration of the Hertz contact law [48] as well as

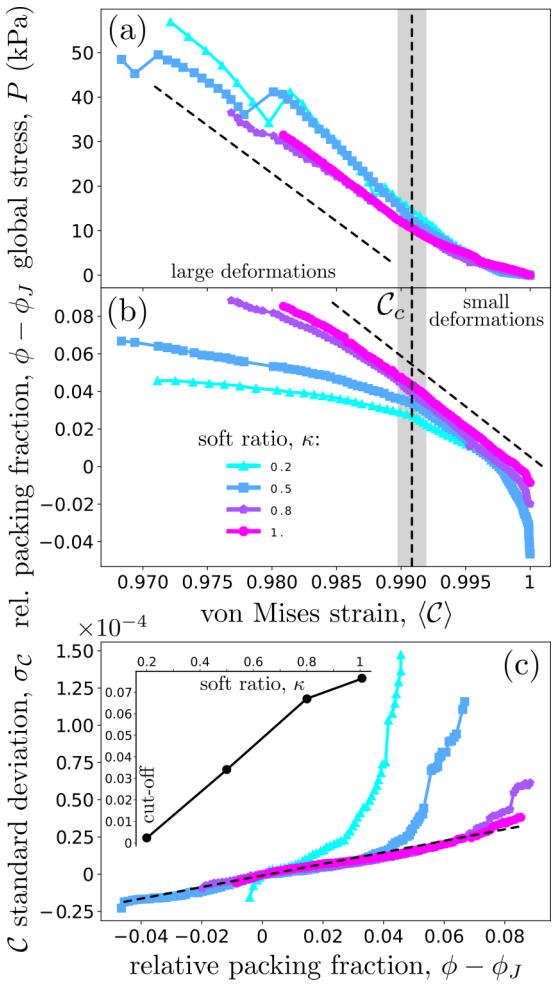

FIG. 4. (a) and (b) Evolution of the global stress P and of the relative packing fraction $\phi - \phi_J$ as a function of the average value of the von Mises strain $\langle \mathcal{C} \rangle$ in soft particles for different κ values, given in the legend in (b) (for the three panels). In (a) and (b), straight black dashed lines show slopes of 2.2 kPa and 5.4, respectively, as a guide for the eyes. The vertical dashed line and the shaded area show the crossover strain $\mathcal{C}_c = 0.991 \pm 1.2 \times 10^{-3}$ and its error bar, respectively. It splits the space horizontally between small and large deformation levels. (c) Evolution of the standard deviation of the von Mises strain in soft particles as a function of the relative packing fraction $\phi - \phi_J$. The straight dashed line with a slope of 4.0×10^{-4} is a fit of the curves collapsed in their linear regime. These curves leave their linear regime at certain cutoff whose approximated values are given in the inset as a function of the softness ratio κ.

the Z vs $\phi - \phi_0$ equation permits us to predict this linear relation [32]. It is important to note that this linearity persists far beyond the small deformation regime and even for any particle mix, which makes it useful to indirectly deduce the packing fraction evolution of a compressed system from the contact geometry observation. In the $\langle a \rangle$ vs P relations, it is remarkable that linear coefficients also increase linearly with the softness ratio, while they remain independent of κ for the $\langle l \rangle$ vs ϕ relation.

Relations between global observables and the local deformation field are also revealed in our experimental results. For a small level of deformation, the average strain inside particles evolves linearly with the packing fraction ($\langle \mathcal{C} \rangle \sim \phi - \phi_J$), while in the case of an important loading, it scales with the global pressure applied to the system ($\langle \mathcal{C} \rangle \sim P$). This evidences two distinct regimes deep in the jammed state, as already observed in [12], separated by a crossover value $\mathcal{C}_c \approx 0.991$ independent of κ. In the first regime, linearity is reminiscent of the fact that the global strain scales with the packing fraction [32], so this seems to be extrapolated to the local strain. In the second regime, linearity between strain and stress suggests that the material behaves like a bulk one (except for small rearrangements); this is consistent with the fact that the material is very dense with almost no interstitial porosity. It is also consistent with the fact that, at large compression levels, the pressure seems to decrease faster with the strain for a lower softness ratio; the material gets stiffer for lower κ. On the contrary, linear relations collapse in the case of small deformations and do not significantly depend on the softness ratio. Finally, a scaling between the strain standard deviation and the packing fraction is evidenced ($\sigma_{\mathcal{C}} \sim \phi - \phi_J$) and does not depend on the softness ratio. Only the linearity cutoff increases with κ. This is explained by the fact that for low κ soft particles deform more and more rapidly, entering faster in a nonlinear regime.

Granular systems composed of purely soft or mixed rigidity particles are ubiquitous, so we believe that the results obtained in this Letter, more specifically the compaction law and scaling relations, can release blockages in domains as different as biology, geoscience, and industry. Using our experimental setup, these results could be extended to the case of noncircular particles or the case of a mixture of particles with different rheologies.

Acknowledgments. We thank G. Camp and S. Devic for their technical help with the experimental setup and the particle making process.

[1] T. P. J. Wyatt, A. R. Harris, M. Lam, Q. Cheng, J. Bellis, A. Dimitracopoulos, A. J. Kabla, G. T. Charras, and B. Baum, Emergence of homeostatic epithelial packing and stress dissipation through divisions oriented along the long cell axis, Proc. Natl. Acad. Sci. USA **112**, 5726 (2015).

[2] J. Mauer, S. Mendez, L. Lanotte, F. Nicoud, M. Abkarian, G. Gompper, and D. A. Fedosov, Flow-Induced Transitions of Red Blood Cell Shapes under Shear, Phys. Rev. Lett. **121**, 118103 (2018).

[3] F. Bolton and D. Weaire, Rigidity Loss Transition in a Disordered 2D Froth, Phys. Rev. Lett. **65**, 3449 (1990).

[4] G. Katgert and M. van Hecke, Jamming and geometry of two-dimensional foams, Europhys. Lett. **92**, 34002 (2010).

[5] J. Brujić, S. F. Edwards, D. V. Grinev, I. Hopkinson, D. Brujić, and H. A. Makse, 3D bulk measurements of the force distribution in a compressed emulsion system, Faraday Discuss. **123**, 207 (2003).

[6] J. Zhou, S. Long, Q. Wang, and A. D. Dinsmore, Measurement of forces inside a three-dimensional pile of frictionless droplets, Science **312**, 1631 (2006).

[7] J. A. Cooper and L. E. Eaton, Compaction behavior of several ceramic powders, J. Am. Ceram. Soc. **45**, 97 (1962).

[8] K. Kawakita and K.-H. Lüdde, Some considerations on powder compression equations, Powder Technol. **4**, 61 (1971).

[9] A. J. Liu and S. R. Nagel, Jamming is not just cool any more, Nature (London) **396**, 21 (1998).

[10] N. W. Hayman, L. Ducloué, K. L. Foco, and K. E. Daniels, Granular controls on periodicity of stick-slip events: Kinematics and force-chains in an experimental fault, Pure Appl. Geophys. **168**, 2239 (2011).

[11] J. Barés, D. Wang, D. Wang, T. Bertrand, C. S. O'Hern, and R. P. Behringer, Local and global avalanches in a two-dimensional sheared granular medium, Phys. Rev. E **96**, 052902 (2017).

[12] T.-L. Vu and J. Barés, Soft-grain compression: Beyond the jamming point, Phys. Rev. E **100**, 042907 (2019).

[13] H. Jacquin, L. Berthier, and F. Zamponi, Microscopic Mean-Field Theory of the Jamming Transition, Phys. Rev. Lett. **106**, 135702 (2011).

[14] M. van Hecke, Jamming of soft particles: Geometry, mechanics, scaling and isostaticity, J. Phys.: Condens. Matter **22**, 033101 (2010).

[15] A. Zaccone and E. Scossa-Romano, Approximate analytical description of the nonaffine response of amorphous solids, Phys. Rev. B **83**, 184205 (2011).

[16] F. Radjai, M. Jean, J.-J. Moreau, and S. Roux, Force Distributions in Dense Two-Dimensional Granular Systems, Phys. Rev. Lett. **77**, 274 (1996).

[17] C. S. O'Hern, L. E. Silbert, A. J. Liu, and S. R. Nagel, Jamming at zero temperature and zero applied stress: The epitome of disorder, Phys. Rev. E **68**, 011306 (2003).

[18] T. S. Majmudar, M. Sperl, S. Luding, and R. P. Behringer, Jamming Transition in Granular Systems, Phys. Rev. Lett. **98**, 058001 (2007).

[19] M. Cox, D. Wang, J. Barés, and R. P. Behringer, Self-organized magnetic particles to tune the mechanical behavior of a granular system, Europhys. Lett. **115**, 64003 (2016).

[20] L. Papadopoulos, J. G. Puckett, K. E. Daniels, and D. S. Bassett, Evolution of network architecture in a granular material under compression, Phys. Rev. E **94**, 032908 (2016).

[21] P. Jop, Y. Forterre, and O. Pouliquen, A constitutive law for dense granular flows, Nature (London) **441**, 727 (2006).

[22] M. Cárdenas-Barrantes, D. Cantor, J. Barés, M. Renouf, and E. Azéma, Compaction of mixtures of rigid and highly deformable particles: A micromechanical model, Phys. Rev. E **102**, 032904 (2020).

[23] M. Cárdenas-Barrantes, D. Cantor, J. Barés, M. Renouf, and E. Azéma, Micromechanical description of the compaction of soft pentagon assemblies, Phys. Rev. E **103**, 062902 (2021).

[24] M. Cárdenas-Barrantes, D. Cantor, J. Barés, M. Renouf, and E. Azéma, Three-dimensional compaction of soft granular packings, Soft Matter **18**, 312 (2022).

[25] D. Cantor, M. Cárdenas-Barrantes, I. Preechawuttipong, M. Renouf, and É. Azéma, Compaction Model for Highly Deformable Particle Assemblies, Phys. Rev. Lett. **124**, 208003 (2020).

[26] B. Indraratna, Y. Qi, T. N. Ngo, C. Rujikiatkamjorn, T. Neville, F. B. Ferreira, and A. Shahkolahi, Use of geogrids and recycled rubber in railroad infrastructure for enhanced performance, Geosciences **9**, 30 (2019).

[27] H. Khatami, A. Deng, and M. Jaksa, The arching effect in rubber–sand mixtures, Geosynth. Int. **27**, 432 (2020).

[28] H.-H. H.-H.Tsang, Seismic isolation by rubber–soil mixtures for developing countries, Earthquake Eng. Struct. Dyn. **37**, 283 (2008).

[29] A. Tsiavos, N. A. Alexander, A. Diambra, E. Ibraim, P. J. Vardanega, A. Gonzalez-Buelga, and A. Sextos, A sand-rubber deformable granular layer as a low-cost seismic isolation strategy in developing countries: Experimental investigation, Soil Dyn. Earthquake Eng. **125**, 105731 (2019).

[30] A. Anastasiadis, K. Senetakis, and K. Pitilakis, Small-strain shear modulus and damping ratio of sand-rubber and gravel-rubber mixtures, Geotech. Geol. Eng. **30**, 363 (2012).

[31] M. S. Mashiri, J. S. Vinod, M. N. Sheikh, and H. H. Tsang, Shear strength and dilatancy behaviour of sand–tyre chip mixtures, Soils Found. **55**, 517 (2015).

[32] See Supplemental Material at http://link.aps.org/supplemental/10.1103/PhysRevE.106.L022901 for more details about the uniaxial compaction model for mixed granular systems, the way to select the packing fraction ϕ_j at the jamming transition and the corresponding mean coordination number z_j, how to derive the linear evolution of the average contact length with the packing fraction, the tensorial computation in the nonlinear elasticity theory, and a figure showing the evolution of the von Mises strain probability density function (pdf).

[33] J. Barés, M. Cárdenas-Barrantes, D. Cantor, É. Azéma, and M. Renouf, Highly strained mixtures of bidimensional soft and rigid grains: An experimental approach from the local scale, EPJ Web Cofn. **249**, 05004 (2021).

[34] Canon CanoScan 9000f Mark II.

[35] Moldstar 15 Slow, castable silicone from Smooth-On, https://www.smooth-on.com/products/mold-star-15-slow/.

[36] T.-L. Vu, J. Barés, S. Mora, and S. Nezamabadi, Numerical simulations of the compaction of assemblies of rubberlike particles: A quantitative comparison with experiments, Phys. Rev. E **99**, 062903 (2019).

[37] T.-L. Vu, J. Barés, S. Mora, and S. Nezamabadi, Deformation field in diametrically loaded soft cylinders, Exp. Mech. **59**, 453 (2019).

[38] PYTHON codes to postprocess experimental images (particle tracking, DIC, field computation, etc.), https://git-xen.lmgc.univ-montp2.fr/Image/granular_dic.

[39] L. A. Taber, *Nonlinear Theory of Elasticity: Applications in Biomechanics* (World Scientific, Singapore, 2004).

[40] D. Wang, J. Ren, J. A. Dijksman, H. Zheng, and R. P. Behringer, Microscopic Origins of Shear Jamming for 2D Frictional Grains, Phys. Rev. Lett. **120**, 208004 (2018).

[41] D. S. Bassett, E. T. Owens, K. E. Daniels, and M. A. Porter, Influence of network topology on sound propagation in granular materials, Phys. Rev. E **86**, 041306 (2012).

[42] E. Azéma, F. Radjai, and G. Saussine, Quasistatic rheology, force transmission and fabric properties of a packing of irregular polyhedral particles, Mech. Mater. **41**, 729 (2009).

[43] B. Andreotti, Y. Forterre, and O. Pouliquen, *Granular Media: Between Fluid and Solid* (Cambridge University Press, Cambridge, 2013).

[44] S. Nezamabadi, X. Frank, J.-Y. Delenne, J. Averseng, and F. Radjai, Parallel implicit contact algorithm for soft particle systems, Comput. Phys. Commun. **237**, 17 (2019).

[45] N. Estrada, A. Taboada, and F. Radjai, Shear strength and force transmission in granular media with rolling resistance, Phys. Rev. E **78**, 021301 (2008).

[46] A. E. Skinner, A note on the influence of interparticle friction on the shearing strength of a random assembly of spherical particles, Geotechnique **19**, 150 (1969).

[47] L. Rothenburg and R. J. Bathurst, Analytical study of induced anisotropy in idealized granular materials, Geotechnique **39**, 601 (1989).

[48] L. D. Landau and E. M. Lifshitz, *Theory of Elasticity*, Course of Theoretical Physics Vol. 7 (Pergamon, Oxford New York, 1986).